Impact of composite soft-rigid elastic projectiles: A numerical study

Christophe D'Angelo [1], Guillaume Giombini [1], Franck Celestini [1,*] and Christophe Raufaste [1,2,†]

[1]*Université Côte d'Azur, CNRS, Institut de Physique de Nice, 06200 Nice, France*
[2]*Institut Universitaire de France (IUF), 75005 Paris, France*

We study by numerical simulation the impact of a one-dimensional composite projectile, composed of two superposed homogeneous parts, on an infinitely rigid and massive wall. The coefficient of restitution and the contact time are systematically measured as functions of the contrasts of mass and stiffness between the two parts. For purely elastic parts, these quantities show complex trends associated with different dynamics of the deformation waves propagating inside the projectile. A significant portion of the initial kinetic energy can be trapped in the deformation modes: the coefficient of restitution is lowest, about 0.2, when there is a strong stiffness contrast between the two parts and the stiff and soft parts are at the leading and trailing edges of the projectile respectively. In this case, we highlight the presence of multiple bounces, whose number increases as the proportion of the soft part increases. Finally, viscoelastic parts can be implemented in the same numerical framework to successfully recover the results obtained in real composite projectile impact experiments [D'Angelo *et al.*, Phys. Rev. E **103**, 053005 (2021)].

I. INTRODUCTION

If an impact between two objects is known to conserve momentum, it is not always the case of the translational kinetic energy of the system. Energy can be dissipated or transmitted to other forms of energy as expected in inelastic collisions [1]. There are evidences that systems driven by conservative forces can lead to bad restitution due to a significant amount of the initial kinetic energy spread among the internal modes of the system. This is the case at the microscopic level with impacts of clusters of particles: they can generate transiently very high pressure, density and temperature conditions and activate chemical reactions [2–5]. At the macroscopic level, the lost of the initial translational kinetic energy of a system is quantified by the coefficient of restitution $e = v_a/v_b$ defined as the ratio of the relative speed after impact to the relative speed before impact. If we consider the case of the impact of homogeneous elastic objects, such as spheres and disks, with a very rigid and massive wall, the coefficient of restitution remains close to 1 as long as the impact velocity v_b is small compared to the speed of sound c [6–10]. This is what observed Falcon *et al.* [11] in experiments with centimetric tungsten carbide beads impacting an aluminium wall at typically 0.01 m s^{-1}.

The case of heterogeneous projectiles seems particular. In the simplest geometry of 1D elastic solids, the coefficient of restitution equals one except at high impact speed if unharmonic effects are accounted for [12–14]. Basile and Dumont [13] have shown in simulation that the introduction of a softer part at the leading edge of 1D elastic chains can decrease significantly the coefficient of restitution, around 0.6, even for

harmonic solids. In experiments, D'Angelo *et al.* [15] have shown that cylindrical projectiles made of the superposition of a soft part on top of a rigid one can have a very low coefficient of restitution, around 0.2, although the impact speed remains very low and the two parts are rather elastic taken separately. These results found an echo with the work of Ruan and Yu [16] who found strong variations of the coefficient of restitution with a two-degree-of-freedom mass-spring system depending on the parameters. These bicomposite projectiles seem to have particular energy transmission properties in other situations for which they are accelerated [17,18].

The goal of this paper is twofold. We first consider a 1D harmonic solid with a contrast of elastic modulus between the upper and lower parts that is systematically varied. In particular, we look for the optimal configuration to decrease the coefficient of restitution and favor the transfer of energy to the internal modes of deformation, which is obtained with the soft-on-top configuration. In this configuration, we highlight the presence of multiple bounces, whose number increases with the stiffness contrast and the proportion of soft material. Second, to rationalize the experimental results of D'Angelo *et al.* obtained with the soft-on-top configuration [15,19], viscoelastic parts are implemented with the same numerical framework. The simulations are in very good agreement with the experimental data without any fitting parameters and allow to rationalize an empirical factor used until now.

II. BASIC EQUATIONS

The deformation dynamics is described by the one-dimensional momentum balance or wave equation for the displacement field $u(y, t)$ [20]:

$$\rho(y)\partial_{tt}^2 u(y, t) = \partial_y[E(y)\partial_y u(y, t) + \eta(y)\partial_y\partial_t u(y, t)]. \quad (1)$$

*Corresponding author: franck.celestini@univ-cotedazur.fr
†Corresponding author: christophe.raufaste@univ-cotedazur.fr

Here $y \in [0, L]$ is the position, oriented upward, inside the undeformed linear projectile of length L. $\rho(y)$, $E(y)$, and $\eta(y)$ are the local density, Young modulus and viscosity respectively. This equation accounts for the rheology of a Kelvin-Voigt solid with a local force given by $E \partial_y u + \eta \partial_y \partial_t u$. The dynamics is subject to the following boundary conditions due to the impact at $t = 0$ and velocity v_b with an infinitely massive and rigid wall situated below:

$$
\text{BCs} \begin{cases} u(0, t) &= v_b t \\ \partial_t u(y, 0) &= 0 \\ \partial_y u(y, t) &\xrightarrow{y \to L} 0 \end{cases}.
\tag{2}
$$

In what follows, we consider the case of an heterogeneous projectile composed of two homogeneous parts separated by a sharp interface. Such a bilayered projectile is composed of a part P_1 of length L_1 with parameters ρ_1, E_1, and η_1 at the bottom and of a part P_2 of length L_2 with parameters ρ_2, E_2, and η_2 on top. The interface is located at $y_c = L_1$ and the displacement dynamics is driven by the equation

$$
\frac{1}{c_i^2} \partial_{tt}^2 u = \partial_{yy}^2 u + \tau_i \partial_{yyt}^3 u,
\tag{3}
$$

with $c_i = \sqrt{E_i/\rho_i}$ the wave speed and $\tau_i = \eta_i/E$ the viscoelastic relaxation time in part $i = 1$ or 2. There is an additional boundary condition,

$$
E_1 \partial_{y^-} u(y_c, t) + \eta_1 \partial_{y^- t}^2 u(y_c, t) = E_2 \partial_{y^+} u(y_c, t) + \eta_2 \partial_{y^+ t}^2 u(y_c, t),
\tag{4}
$$

to account for the continuity of the force at the interface $y = y_c$. In what follows, we consider $\rho_1 = \rho_2 = \rho$ so that the composition factor $x = L_2/(L_1 + L_2) = m_2/(m_1 + m_2)$ represents the ratio between the length/mass of the top part and the total length/mass. With the same idea, we note $\alpha = E_2/(E_1 + E_2)$ the stiffness ratio.

In this approach, the coefficient of restitution e is directly associated with the deformation at $y = 0$, $\varepsilon_0(t) = \partial_y u(0, t)$. If the projectile takes off at t_c, the takeoff velocity v_a of the center of mass writes

$$
v_a = -v_b - \frac{E_1}{\rho(L_1 + L_2)} \int_0^{t_c} \varepsilon_0(t) dt
$$
$$
- \frac{\eta_1}{\rho(L_1 + L_2)} \int_0^{t_c} \dot{\varepsilon}_0(t) dt
\tag{5}
$$

following the integration of Newton's second $\rho(L_1 + L_2) \frac{dv}{dt}(t) = -E_1 \varepsilon_0(t) - \eta_1 \dot{\varepsilon}_0(t)$, with v the velocity of the center of mass. Gravity is neglected in this equation, which is valid as long as $g t_c / v_b \ll 1$ with g the standard gravity. Given that $\varepsilon_0(0) = \varepsilon_0(t_c) = 0$, this leads to

$$
e = -1 - \frac{c_1^2}{(L_1 + L_2)v_b} \int_0^{t_c} \varepsilon_0(t) dt.
\tag{6}
$$

Note that it is possible for a projectile to reconnect to the wall after a first takeoff. Consequently, we might observe successive stages of reconnection and separation between 0 and t_c. The contact time t_c is thus defined as the time of the last contact with the wall.

III. NUMERICAL IMPLEMENTATION

The projectile consists of a one-dimensional chain of N masses m connected to each other by an elastic spring in parallel to a viscous damper (Fig. 1). The equilibrium length of the springs is noted l_0; the elastic and viscous constants are noted k_i and k_i' with $i = 1$ and 2 in the parts P_1 and P_2, respectively. The chain is composed of N_1 elements (k_1, k_1') superposed by N_2 elements (k_2, k_2'). The link between the microscopic parameters of the discrete approach and the physical parameters of Eq. (3) are easily established: the wave speeds velocities and viscoelastic relaxation times write $c_i = \sqrt{k_i l_0^2/m}$ and $\tau_i = k_i'/k_i$. With this discrete approach the composition and stiffness ratios write $x = N_2/(N_1 + N_2)$ and $\alpha = k_2/(k_1 + k_2)$. In what follows, all displayed quantities are dimensionless so that we take $m = 1$, $l_0 = 1$ and $k_1 + k_2 = 1$ without loss of generality. In practice, both x and α are varied in the interval $[0.005 ; 0.995]$ with steps $\Delta x = \Delta \alpha = 0.005$. The total number of elements $N = N_1 + N_2$ is kept constant and equal to 10^4, a number large enough to neglect finite size effects (Appendix A). The position $y_j(t)$ of a mass j follows the second law of Newton: $m \ddot{y}_j(t) = -F_{j,j-1}(t) + F_{j+1,j}(t)$ with $F_{j,j-1} = k_i(y_j - y_{j-1} - l_0) + k_i'(\dot{y}_j - \dot{y}_{j-1})$ the viscoelastic force exerted by mass j on mass $j - 1$. With our notations, (k_i, k_i') equals (k_1, k_1') or (k_2, k_2') if the mass j is in part P_1 or in P_2, respectively. This relation is modified on the edges of the projectile. At the upper end, the mass N follows $m \ddot{y}_N(t) = -F_{N,N-1}(t)$, while at the lower end, the expression of the force is modified whether the projectile is in contact or not with the wall situated at $y_0 = 0$. If the projectile is not in contact ($y_1 > l_0$), $m \ddot{y}_1(t) = F_{2,1}(t)$, while the contact force $-F_{1,0}(t)$ is added in case of contact with the wall ($y_1 < l_0$). Initially, each mass j of the chain is separated by the distance l_0 from its neighbors and has a velocity $-v_b$: $y_j(0) = j l_0$ and $\dot{y}_j(0) = -v_b$ for $j \in [1; N]$. The dynamics of the system is solved with the Beeman algorithm [21]. To ensure precise results within the numerical approach, simulation parameters need to be adjusted. First, the time step dt between two iterations needs to be smaller than the smallest physical time of the system. We took $dt = \min(2\pi\sqrt{m/k_1}, 2\pi\sqrt{m/k_2})/100$. Second, the total simulation time must be larger than the largest physical time. If we note $t_i = N_i l_0/c_i$ the time for the fastest deformation wave to travel through part P_i, the simulation is stopped after a total time equal to $\max(t_1, t_2) * 20$. Finally the impact velocity must remain significantly smaller than the deformation speeds and we took $v_b = \min(c_1, c_2)/200$. As observed in experiments [15], the dynamics can exhibit successive stages of reconnection and separation. To quantify the intermediate bounces, we note N_b the total number of stages, with $N_b = 1$ the classical case of a single rebound. Finally, the velocity after impact is obtained with the expression $v_a = \frac{1}{N} \sum_{j=1}^{N} \dot{y}_j(t_c)$. The software VMD is used for visualization of the position of each mass [22]. For ease of observation, we choose $N = 100$ and duplicated the chain in order to represent four identical chains next to each other. Each mass has a color corresponding to the deformation $\varepsilon_j = \frac{(y_j - y_{j-1}) - l_0}{l_0}$ of the associated spring. In Fig. 1(b), we observe such an image sequence obtained with VMD. The projectile is first represented before the impact (image 1). The masses have a white color corresponding to a spring at rest. After
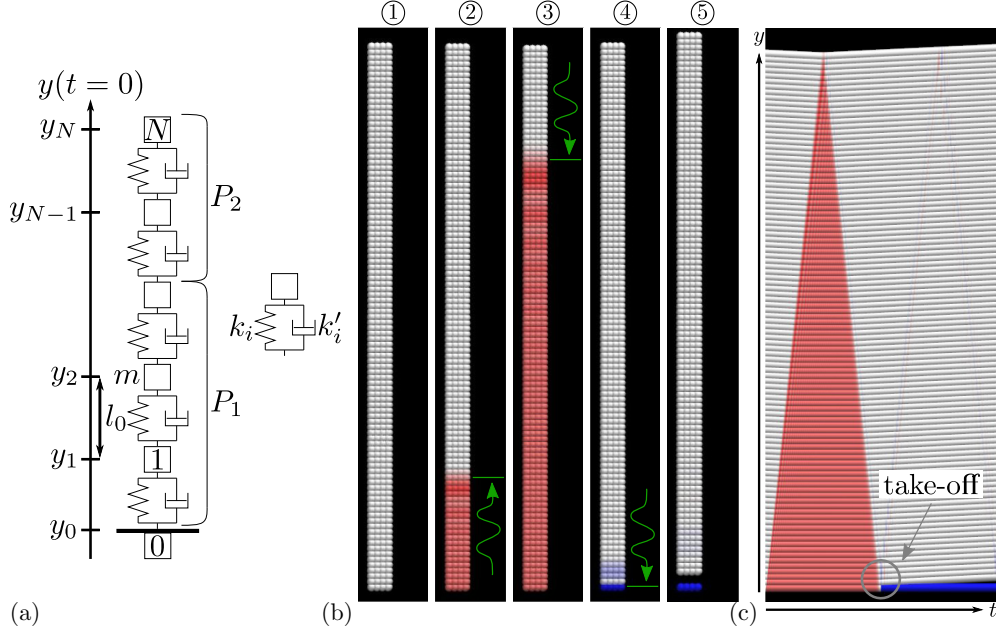
FIG. 1. (a) Diagram of a mass-spring chain with $N = 5$ and $x = 0.4$. (b) Image sequence and (c) space-time diagram of an homogeneous projectile ($\alpha = 0.5$) with $N = 100$ highlighting the propagation of a deformation wave, whose front position and propagation direction are indicated by a green arrow. The white color indicates no deformation. The red, respectively blue, color indicates a negative, respectively positive, deformation.

the impact (image 2), a compression wave starts propagating in the chain. Its direction is indicated by a green arrow and the masses are displayed in red corresponding to a negative deformation. At some point, the wave reaches the top of the projectile and is reflected downwards (image 3). The masses then turn white following a relaxation wave that resets the deformation to 0. This wave finally reaches the bottom of the projectile (image 4) and the mass 0 (the wall) becomes blue. The blue color corresponds to an elongation of the spring, except for the mass 0 where it indicates that the projectile is no longer in contact with the wall. Finally, the projectile takes off (image 5) and all the masses are white which means that no energy is trapped in the deformation modes of the projectile as expected for a homogeneous 1D chain. In Fig. 1(c), the space-time diagram obtained from the VMD image sequence allows an easy representation of the full dynamics. The gray circles indicate the takeoff time and the intermediate stages of reconnection and separation if any.

IV. RESULTS FOR HOMOGENEOUS PROJECTILES

Inside an homogeneous projectile, Eq. (3) reduces to

$$\partial_{tt}^2 u = c^2 \partial_{yy}^2 u + c^2 \tau \partial_{yyt}^3 u \qquad (7)$$

with $c = \sqrt{E/\rho}$ the wave speed and $\tau = \eta/E$ the viscoelastic relaxation time. Any physical parameter is therefore a function of c, τ, L and v_b only. Given that the system is linear, the takeoff velocity is proportional to v_b and the coefficient of restitution e is only a function of the dimensionless number $\tau c/L$. The coefficient of restitution of a homogeneous projectile is obtained following the numerical approach introduced in Sec. III. In Fig. 2(a), we observe that e decreases from 1 to 0 as $\tau c/L$ increases from 0 to 1 following the trend

$1 - e \simeq (\tau c/L)^{1/2}$. We can gain some intuition by looking at the deformation dynamics $\varepsilon_0(t)$ at the contact. Following Eq. (6), the coefficient of restitution of an homogeneous projectile writes

$$e = -1 - \frac{c^2}{Lv_b} \int_0^{t_c} \varepsilon_0(t) dt. \qquad (8)$$

This expression shows that the coefficient of restitution depends on the area under the curve $\varepsilon_0(t)$. For a material with negligible dissipation ($\tau \ll L/c$), the contact time t_c corresponds to $2L/c$ the time for the wave to go back and forth inside the projectile and $\varepsilon_0(t) = -v_b/c$ during this time interval [1]. As a consequence $\int_0^{t_c} \varepsilon_0(t) dt = -2\frac{Lv_b}{c^2}$ and $e = 1$. If dissipation needs to be accounted for, $\varepsilon_0(t)$ needs two finite times to go from 0 to $-v_b/c$ and from $-v_b/c$ to 0 during the initial/final stages of the impact [Fig. 2(b)]. The first time is proportional to the viscoelastic relaxation time τ. The second time is quantified by the duration t_ε for ε_0 to vary from $-v_b/2c$ to 0 and is found to vary as $t_\varepsilon \propto (\tau L/c)^{1/2}$ [insert of Fig. 2(b)]. The second time is thus the largest in the limit $\tau \ll L/c$ as illustrated in Fig. 2(b). As a consequence, the deviation of the coefficient of restitution from 1 is proportional to $t_\varepsilon c/L$ in this limit, $1 - e \propto t_\varepsilon c/L$, which retrieves the result found with the numerical approach. We give a simple argument to explain the scaling obtained for t_ε. The two terms in the right side of Eq. (7) have a different physical meaning. The first is associated with the propagation of waves at speed c and the second with a diffusive process and a diffusion coefficient $c^2\tau$. In the limit $\tau \ll L/c$, the propagation term is dominant at the leading order approximation which results in the propagation at speed c of a sharp perturbation front following the impact with the wall. The diffusive term has a second order
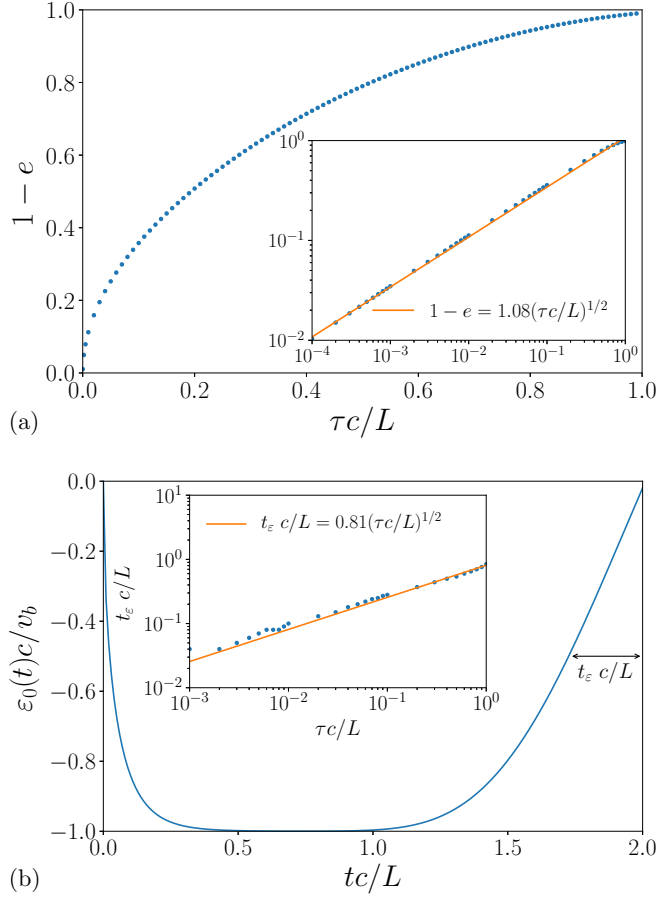
FIG. 2. (a) $1 - e$ as a function of $\tau c/L$ for an homogeneous projectile (blue dots). Inset: same data (blue dots) in a logarithmic scale and best fit (yellow solid line) obtained by applying a power law with an exponent 1/2. (b) Rescaled deformation at the contact $\varepsilon_0(t)c/v_b$ as a function of the dimensionless time tc/L for a simulation with $\tau c/L = 0.1$ (solid line). Insert: $t_\varepsilon c/L$ as a function of $\tau c/L$ in a logarithmic scale (blue dots) and best fit (yellow solid line) obtained by applying a power law with an exponent 1/2.

effect that broadens the width of the propagation front. If we call w this width, we expect $w(t) \propto \sqrt{c^2 \tau t}$. At the takeoff time $t_c \simeq 2L/c$, the perturbation front went back and forth in the projectile and its width equals $w(t_c) \propto \sqrt{\tau L c}$. This leads to a typical duration $w(t_c)/c \propto \sqrt{\tau L/c}$ for the deformation at contact to relax in agreement with the scaling measured for t_ε.

V. RESULTS FOR ELASTIC BILAYERED PROJECTILES

In this section, we focus on perfectly elastic bilayered projectiles ($\tau_1 = \tau_2 = 0$) and study systematically the contact time t_c, the total number of bounces N_b and the coefficient of restitution e as functions of the composition and rigidity ratios x and α. With our notations, the time to travel trough part P_1, respectively P_2, is written $t_1 = L_1/c_1$, respectively $t_2 = L_2/c_2$.

A. Typical dynamics

In Fig. 3, we have displayed space-time diagrams for several values of x and α. For each of them, we see the initial

compression front propagating from the bottom-left corner, the reflection/transmission at the P_1-P_2 interface followed by successive events. In all cases, we observe propagation back and forth inside both parts with reflections at $y = 0$ and $y = L_1 + L_2$, and refraction at $y = y_c$, whose order of events depends on x and α. When the deformation at contact ε_0 equals 0, the projectile takes off. The takeoff might be definitive [Figs. 3(a), 3(b), and 3(d)] or several stages of reconnection/separation can be observed [Fig. 3(c)].

B. Contact time

For the case of an homogeneous, linear and purely elastic projectile, the contact time is given by the time for the deformation wave to travel back and forth inside the object (Sec. IV). To compare the results with this reference case, we define the dimensionless contact time $\tilde{t}_c = t_c/(2t_1 + 2t_2)$. In Fig. 4(a), we observe that $\tilde{t}_c = 1$ for a large range of α regardless of the value of x. Deviations are observed only for strong differences in elastic modulus, typically $\alpha \lesssim 0.1$ or $\alpha \gtrsim 0.8$. For $\alpha \lesssim 0.1$, $\tilde{t}_c < 1$ is mainly observed for $x < 0.4$ where inertia of the lower and more rigid part dominates. In this region, the contact time is shorter than $2t_1 + 2t_2$. This means that the projectile bounces before the deformation wave propagating through the upper and softer part is coming back to the contact zone. In practice, this means that the dynamics is strongly dominated by the properties of the lower and more rigid part and that the contact time should be a multiple of $2t_1$, the time for a deformation wave to travel inside the lower part. Indeed, we observe that this region is well characterized by $t_c = 2t_1$ with a single travel through the lower part [Fig. 3(a)]. For $\alpha \gtrsim 0.8$, $\tilde{t}_c > 1$ regardless of x and the strongest variations to the reference case are observed in the top/right corner of the $(x; \alpha)$ diagram where inertia of the upper and more rigid part dominates. As seen in the image sequence of Fig. 3(d), such cases exhibit dynamics with multiple wave travels inside the lower part and only one single travel inside the upper part (for this example, there are two travels back and forth inside the lower part). From this observation, we suggest to define n_1 from $t_c = n_1 t_1 + 2t_2$ to quantify the number of travels inside the lower and softer part. In Fig. 4(b), we observe that the larger x and α, the higher n_1 and that this quantity takes mainly even values 4, 6, 8,... consistent with the hypothesis of multiple travels inside the lower part. In the top/left corner n_1 is not an integer and takes values in the range [2; 4]. In this case, the dynamics is more complex and several wave travels inside the upper part occur as well.

C. Number of bounces

The study allows a full characterization of multiple bounces that occur in certain cases before the projectile definitively leaves the wall [e.g., in Fig. 3(c)]. This measurement is very sensitive to numerical artifacts that trigger fast changes in the sign of $\varepsilon_0(t)$ when this quantity is small, in absolute value, with respect to v_b/c. Only relevant bounces are recorded by setting the criterion that the time between a separation event and a reconnection event must be greater than $\min(t_1, t_2)$, the minimum physical time for a given set of parameters. The number of bounces N_b as a function of x and α is plotted in
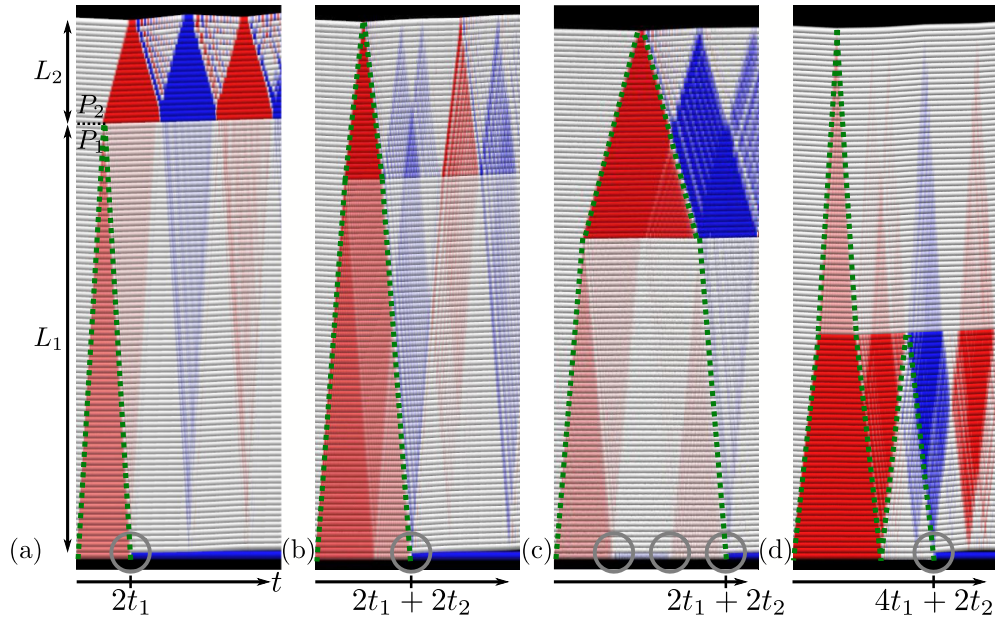
FIG. 3. Space-time diagrams that illustrate the dynamics with (a) $x = 0.2$, $\alpha = 0.05$, and $t_c = 2t_1$; (b) $x = 0.3$, $\alpha = 0.3$, and $t_c = 2t_1 + 2t_2$; (c) $x = 0.4$, $\alpha = 0.05$, and $t_c = 2t_1 + 2t_2$; (d) $x = 0.6$, $\alpha = 0.8$, and $t_c = 4t_1 + 2t_2$. The solid gray circles indicate the separation or reconnection events. The green dotted lines indicate the path of the deformation wave that triggers the final takeoff. In (c), the three solid gray circles indicate the first separation, the reconnection and the final takeoff. In (d), note that between $2t_1 + 2t_2$ and $4t_1 + 2t_2$, the color at the contact is not white but very light red.

Fig. 5. For $\alpha \in [0.2; 0.8]$, N_b equals 1. Associated with $t_c = 2t_1 + 2t_2$, this region remains similar to the reference case of an homogeneous linear object. For $\alpha \in [0.8; 1]$, N_b equals 1 as well. In these two regions, isolated cases associated with $N_b = 2$ are observed but correspond to numerical artifacts. $N_b = 1$ is also retrieved in the bottom/left corner associated with $t_c = 2t_1$. Otherwise, we observe that multiple bounces appear in the bottom/right corner of the $(x; \alpha)$ diagram where t_c is mostly equal to $2t_1 + 2t_2$. Remarkably, N_b increases in this region as x increases or α decreases. Actually this number saturates at $N_b = 5$ but this saturation might be associated to the fact that we do not resolve the bounces if the time between separation/reconnection events becomes smaller than $\min(t_1, t_2)$. In this corner, the lower and rigid part can bounce easily since the soft part on top is not rigid enough to prevent this part from bouncing on a short timescale but still exerts an elastic force that repulses the lower part towards the wall on a larger timescale (but short with respect to t_c) and trigger an additional bounce. This behavior becomes more and more pronounced as the inertia of the lower/rigid part diminishes ($x \to 1$). This behavior is consistent with experiments performed by D'Angelo *et al.* [15] with cylindrical projectiles made of a rigid plastic at the bottom superposed with a soft hydrogel on top: N_b was found to increase as x was increased.

D. Coefficient of restitution

Figure 6(a) displays the coefficient of restitution e as a function of x and α. Again, we can distinguish three regions of interest. In the central region, the coefficient of restitution remains close to one. In the upper region, e can be as low as 0.8. In the lower region, the effect can become very strong and e can be as low as 0.2, a value obtained for $x = 0.4$ and

$\alpha \to 0$. This observation is consistent with experiments and toy models that suggest a minimum restitution with the soft element on top of a rigid element [15,16,19]. In Fig. 6(b), we focus on the lower part of the $(x; \alpha)$ diagram, where variations are the strongest. Plotting e as a function of x for a given α reveals successive line segments, whose number increases and the variations in orientation are more exacerbated as α decreases. As explained in Sec. VI, the positions of the end points between line segments are associated with specific values of traveling time inside the projectiles for $\alpha \simeq 0.5$, while it is also associated with additional stages of reconnection/separation in the limit $\alpha \to 0$. For a given α, we call $e_{\min}$ the minimum value of e and $x_{\min}$ the value associated with this minimum. Both quantities are plotted as a function of α in Fig. 7 for the whole range $\alpha \in [0; 1]$. We noticed that $(x_{\min}, e_{\min})$ corresponds to the first change of slope when e is plotted as a function of x for a given α [Fig. 6(b)].

VI. MODEL FOR ELASTIC BILAYERED PROJECTILES

A. General considerations

The dynamics is intrinsically correlated to the time evolution of the deformation at the contact, $\varepsilon_0(t)$. At $t = 0$, the contact is subject to the compression exerted by the wall and the deformation equals $\varepsilon_i = -v_b/c_1$ [1]. From this instant, a deformation wave travels inside the projectile with a sharp front between the underformed and deformed regions. At $t = t_1$, it reaches the P_1-P_2 interface, which gives rise to a reflected wave of amplitude $R_{12}\varepsilon_i$ traveling at velocity $-c_1$ in P_1 and to a transmitted wave of amplitude $T_{12}\varepsilon_i$ traveling at velocity $+c_2$ in P_2. The reflection and transmission coefficients (R_{12}; T_{12}) for waves traveling from P_1 to P_2 and (R_{21}; T_{21}) for waves traveling from P_2 to P_1 are functions of α only and
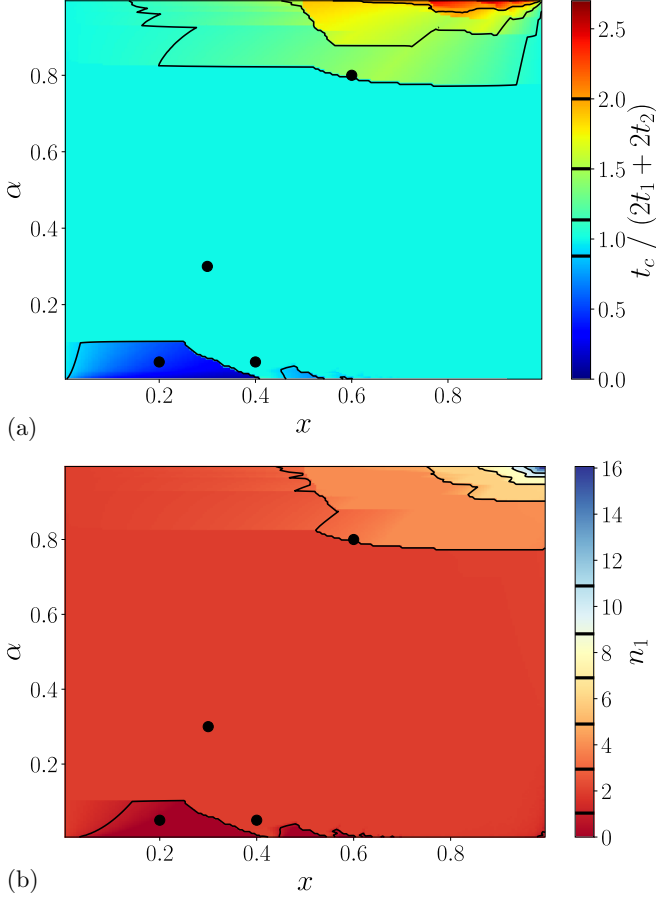
FIG. 4. (a) Dimensionless contact time $\tilde{t}_c = t_c/(2t_1 + 2t_2)$ as a function of x and α. (b) $n_1 = (t_c - 2t_2)/t_1$ as a function of x and α. The black circles indicate the typical cases detailed in Sec. V A. The black lines are isovalue lines whose values are shown in the color bar.

expressed in Appendix B. For $t \in [0; 2t_1[$, $\varepsilon_0(t) = \varepsilon_i$. At $t = 2t_1$, the reflected wave generated at the interface P_1-P_2 at $t = t_1$ reaches the contact zone and modifies the deformation at the contact by adding a component $2R_{12}\varepsilon_i$ and $\varepsilon_0(t \gtrsim 2t_1) = (1 + 2R_{12}(\alpha))\varepsilon_i$. Note that this is only possible if $1 + 2R_{12}(\alpha) \geqslant 0$ so that the contact zone remains in compression. Actually this quantity becomes negative for $\alpha \leqslant 0.1$ and explains what is observed at the bottom of the $(x; \alpha)$ diagram. In this region, the projectile leaves the wall at $t = 2t_1$. In the left part of the $0.1 \leqslant \alpha$ region, $x < 0.25$–0.4, this separation is definitive as characterized by $t_c = 2t_1$ and $N_b = 1$, while in the rest several reconnection/separation stages occur as characterized by $t_c > 2t_1$ (mostly $t_c = 2t_1 + 2t_2$) and $N_b > 1$ (Figs. 4 and 5). If the projectile remains in contact, $\alpha > 0.1$, the state of the contact will change again at $t = 4t_1$ if $t_1 < t_2$ or at $t = 2t_1 + 2t_2$ if $t_1 > t_2$. In the $(x; \alpha)$ diagram, a change of behavior is thus expected for

$$x_1 = \frac{\sqrt{\alpha}}{\sqrt{\alpha} + \sqrt{1 - \alpha}}, \qquad (9)$$

which corresponds to $t_1 = t_2$. If $t_1 < t_2$ $(x > x_1)$, an additional $4R_{12}^2\varepsilon_i$ will contribute to the deformation at the contact associated with an additional reflection of amplitude

$2R_{12}^2$ at the P_1-P_2 interface; in this case $\varepsilon_0(t \gtrsim 4t_1) = (1 + 2R_{12} + 4R_{12}^2)\varepsilon_i$. If $t_1 > t_2$ $(x < x_1)$, the state of the interface is first modified by the wave that has traveled through P_2 and reaches the contact zone at $t = 2t_1 + 2t_2$ with the amplitude $-T_{21}T_{12}\varepsilon_i$; in this case $\varepsilon_0(t \gtrsim 2t_1 + 2t_2) = (1 + 2R_{12} - 2T_{21}T_{12})\varepsilon_i$. Such reasoning is helpful to give insights and understand the results for certain values of x and α. For the rest, the numerical approach is required to deal with the complexity of multiple waves traveling through the material and the description of the separation/reconnection stages. For instance, solving $(1 + 2R_{12} - 2T_{21}T_{12}) = 0$ gives $\alpha = 0.82$ as marked by a transition in the top-left of the $(x; \alpha)$ diagram (limit of the region $t_c = 2t_1 + 2t_2$ with $x < x_1$).

B. Central region $0.1 \leqslant \alpha \lesssim 0.8$

Such simple reasoning can be used to understand what happens in the central region $0.1 \leqslant \alpha \lesssim 0.8$, characterized by $t_c = 2t_1 + 2t_2$ and no additional reconnection/separation stage [Fig. 3(b)]. If $t_1 > t_2$ or $x < x_1$, $\varepsilon_0(t)$ equals ε_i between 0 and $2t_1$ and $(1 + 2R_{12})\varepsilon_i$ between $2t_1$ and $2t_1 + 2t_2$. If $t_1 < t_2$, the state will depend on the number of travels of the waves inside P_1 and the subsequent modification of the deformation at the contact before t_c and separation from the wall. Due to multiple reflections inside the part P_1, the contact deformation is modified every $k * 2t_1$ with $k = 1, 2, 3, \ldots$ due to the arrival at the P_1-wall contact of a wave of amplitude $R_{12}^k\varepsilon_i$. The deformation at the contact is thus modified by addition of $2R_{12}^k\varepsilon_i$ due to the rigid boundary condition (Appendix B). This leads to the expression of the contact deformation $\varepsilon_{0,k}$ in the interval $[k * 2t_1; (k + 1) * 2t_1]$

$$\varepsilon_{0,k} = \left(1 + \sum_{i=1}^{k} 2R_{12}^i\right)\varepsilon_i = \left(-1 + \sum_{i=0}^{k} 2R_{12}^i\right)$$

$$\varepsilon_i = \frac{1 + R_{12} - 2R_{12}^{k+1}}{1 - R_{12}}\varepsilon_i. \qquad (10)$$

If we note n the greatest integer less than or equal to t_2/t_1, $n = \text{floor}(t_2/t_1)$, the coefficient of restitution is obtained from Eq. (6) and writes

$$e = -1 - \frac{c_1^2}{(L_1 + L_2)v_b}\left(2t_1 \sum_{k=0}^{n} \varepsilon_{0,k} + 2(t_2 - nt_1)\varepsilon_{0,n+1}\right). \qquad (11)$$

If we note $F_k(\alpha) = \frac{1 + R_{12} - 2R_{12}^{k+1}}{1 - R_{12}}$ and given that $\varepsilon_i = -v_b/c_1$ and $t_2/t_1 = \frac{x\sqrt{1-\alpha}}{(1-x)\sqrt{\alpha}}$, $e(x) = a_n(\alpha)x + b_n(\alpha)$ with the slope a_n and the intercept b_n for a given n, both functions of α such as

$$a_n(\alpha) = -2\left(\sum_{k=0}^{n} F_k\right) + 2nF_{n+1} + 2F_{n+1}(\alpha)\sqrt{\frac{1-\alpha}{\alpha}},$$

$$b_n = -1 + 2\left(\sum_{k=0}^{n} F_k\right) - 2nF_{n+1}.$$

A direct consequence is that for a given α and a given n, e is a linear function of x that changes slope for discrete values x_n
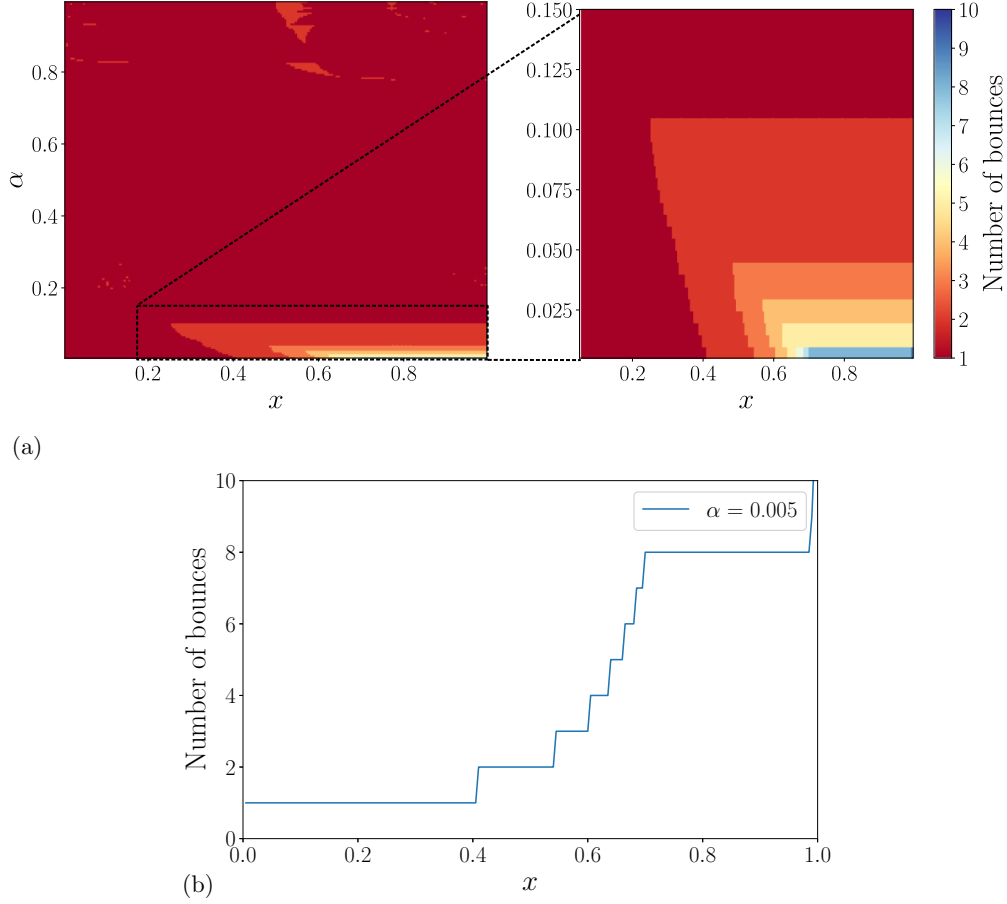
FIG. 5. (a) Number of bounces N_b as a function of x and α: full diagram on the left and enlarged view around the zone of interest on the right. (b) Number of bounces N_b as a function of x for $\alpha \to 0$ ($\alpha = 0.005$).

corresponding to $t_2 = n t_1$:

$$x_n(\alpha) = \frac{n\sqrt{\alpha}}{n\sqrt{\alpha} + \sqrt{1-\alpha}}.$$

This is in agreement with the line segments observed with the numerical approach [Fig. 6(b)] and allows to find expressions of $x_{\min}(\alpha)$ and $e_{\min}(\alpha)$ for α in the central region $0.1 \leqslant \alpha \lesssim 0.8$, given that $x_{\min} = x_1$, $e_{\min} = a_0 x_1 + b_0$, and $F_0 = 1$.

$$x_{\min}(\alpha) = x_1 = \frac{\sqrt{\alpha}}{\sqrt{\alpha} + \sqrt{1-\alpha}}, \tag{12}$$

$$b_0 = 1 \text{ and } a_0(\alpha) = -2\left(1 - F_1(\alpha)\sqrt{\frac{1-\alpha}{\alpha}}\right), \tag{13}$$

$$e_{\min}(\alpha) = e(x_{\min}) = 1 - 2\left(\frac{\sqrt{\alpha} - F_1(\alpha)\sqrt{1-\alpha}}{\sqrt{\alpha} + \sqrt{1-\alpha}}\right). \tag{14}$$

These equations are successful in describing the central region (Fig. 7).

C. Lower region $\alpha \leqslant 0.1$

For $\alpha \lesssim 0.1$, the upper part is significantly softer than the lower part. As a consequence, the reflected wave at the P_1-P_2 interface is poorly modified by the presence of the upper and

softer part so that the projectile takes off at $2t_1$ as expected if part P_1 was alone (Sec. VI A).

For the smallest x, the takeoff is definitive since the upper and softer part is not massive enough to push back the lower part toward the wall. As a consequence, the dynamics is characterized by one single wave travel through the lower and stiffer part and $t_c = 2t_1$ [Fig. 3(a)]. In this case, the deformation at contact equals $\varepsilon_i = -v_b/c$ during the whole impact. From Eq. (6), we deduce that

$$e(x) = 1 - 2x, \tag{15}$$

whatever α in this region in agreement with the results of Fig. 6. This expression is consistent with predictions expected in the limit $\alpha \to 0$, meaning $t_1 \ll t_2$, which considers the lower and stiffer part as a perfectly rigid object that changes velocity on a much shorter timescale than the upper and softer part [19,23]. In this case, the velocity of the rigid part switches from $-v_b$ to v_b following the impact with the wall while the upper and softer part keeps its velocity $-v_b$. The velocity of the center of mass after impact equals $v_a = (1 - x)v_b - xv_b = (1 - 2x)v_b$, which leads to the expression of the coefficient of restitution given by Eq. (15) if no additional reconnection/separation stage occurs.

For intermediate values of x, the upper and softer part is more massive so that it projects again the lower part toward the wall. One or a few additional stages of
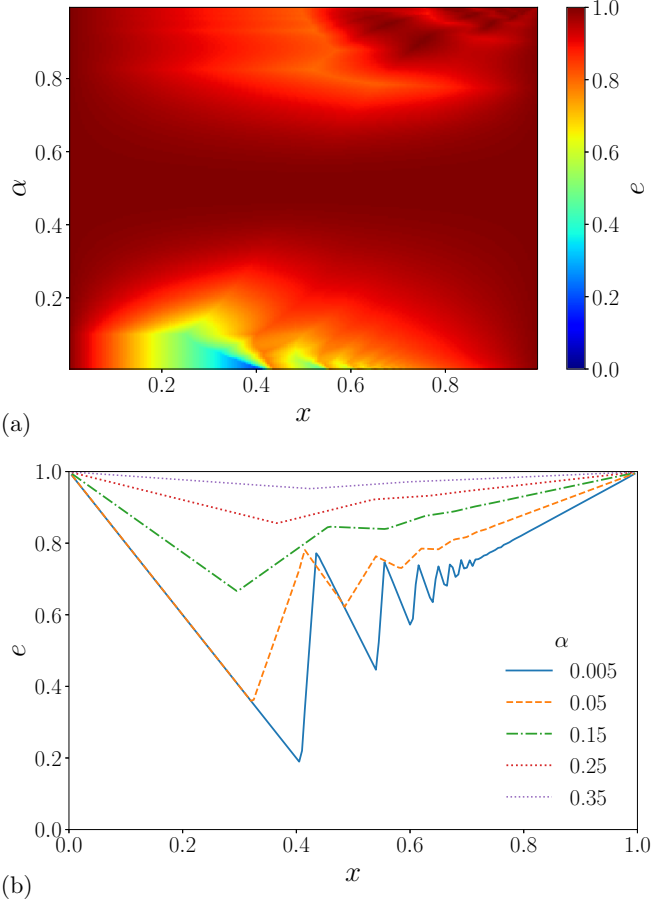
(a)

(b)

FIG. 6. Coefficient of restitution e as a function of x and α. (a) Full diagram. (b) Several profiles for fixed values of $\alpha < 0.5$.

(a)

(b)

FIG. 7. (a) $x_{\min}$ and (b) $e_{\min}$ as functions of α. The solid lines are the expressions expected in the central region $0.1 \leqslant \alpha \lesssim 0.8$, Eqs. (12) and (14).

reconnection/separation occur and the projectile takes off definitively at a time t_c close to $2t_1 + 2t_2$, the time for the wave to travel back and forth through the whole projectile [Fig. 3(c)]. When plotting $e(x)$ as a function of x for a given α [Fig. 6(b)], the positions of the end points between line segments are now both associated with specific values of traveling time inside the projectile and to additional stages of reconnection/separation. The lower α, the larger the slope changes between consecutive line segments. The larger x for a given α, the lower the length of the line segments. In the limit of a perfectly rigid lower part ($\alpha \to 0$), the stages of reconnection/separation are instantaneous and each of them reverses immediately the sign of the velocity of the lower part by an exchange of momentum with the wall. As detailed in Appendix C, the number of such stages in this limit is an increasing and discontinuous function of x. Consequently, the coefficient of restitution is a discontinuous function of x too. Nevertheless, the speed at reconnection decreases with the number of reconnection/separation stages due to the interaction with the upper part so that the exchange of momentum with the wall, and thus the amplitude of the discontinuities in e, decreases as x increases.

For the largest x, the upper and softer part is now significantly more massive than the lower part. A lot of reconnection/separation stages occur and the projectile takes off definitively and exactly at $t_c = 2t_1 + 2t_2$ [Fig. 3(c)]. The
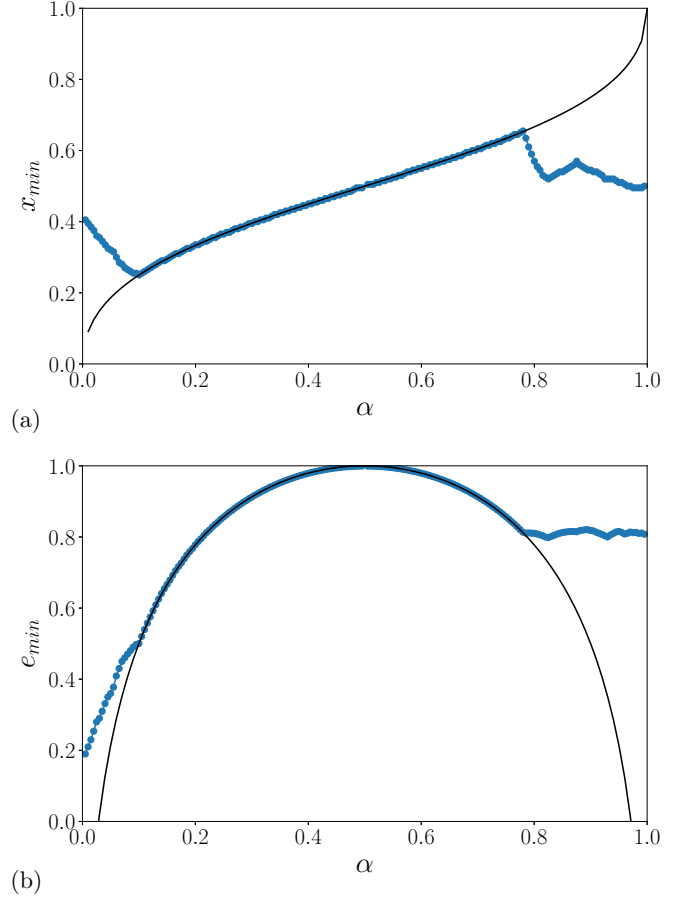
line segments become so small that they appear as one single line that reaches $e = 1$ for $x = 1$ [Fig. 6(b)]. The lower α and the steeper the asymptote, which writes $e(x) = x$ in the limit $\alpha \to 0$. Again we can consider the limit of a perfectly rigid lower part ($\alpha \to 0$). As detailed in Appendix C, for x larger than typically 0.6–0.7, the motion of the lower and rigid part is damped following the multiple exchanges of momentum with the wall and the interaction with the upper part. Consequently, the velocity of the lower part equals 0 at t_c while the upper and softer part has switched its velocity from $-v_b$ to v_b. This retrieves the expression $e(x) = x$ of the simulation results in the limit $\alpha \to 0$ [Fig. 6(b)].

VII. RESULTS FOR VISCOELASTIC BILAYERED PROJECTILES

The case of nondissipative bilayered projectiles was considered in Secs. V and VI. It was obtained by setting $\tau_1 = \tau_2 = 0$ for the viscoelastic relaxation times in both parts P_1 and P_2 or, equivalently, $e_1 = e_2 = 1$ for the coefficients of restitution of each part taken separately. In this section, we now consider the case of viscoelastic bilayered projectiles. In each part P_i, τ_i is now adjusted to fix the coefficient of restitution of the homogeneous projectile of total length L to the desired values e_1 and e_2 (Sec. IV) so that $e(x = 0) = e_1$
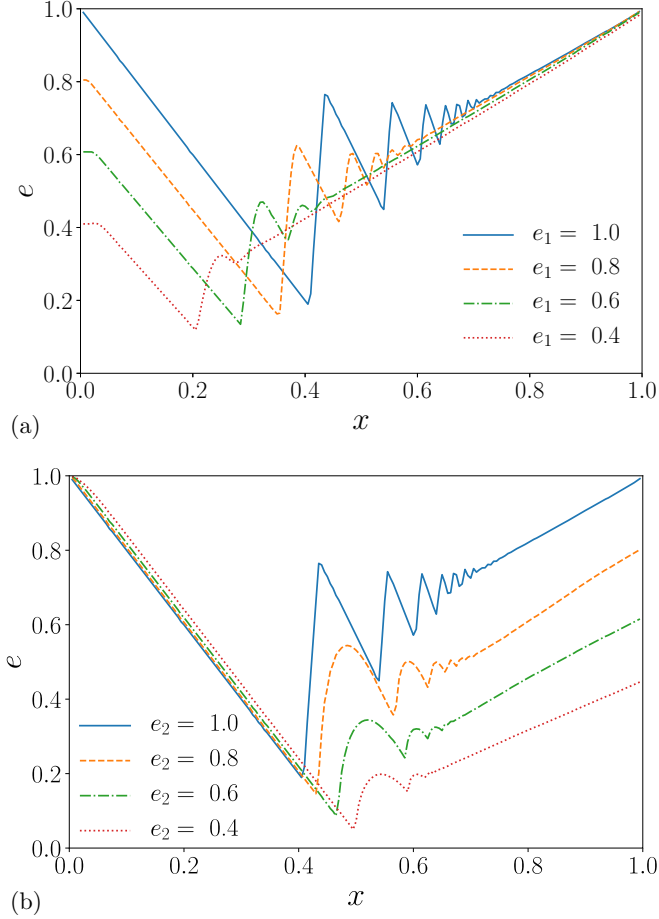
FIG. 8. Coefficient of restitution e as a function of x for $\alpha = 0.005$: (a) $e_2 = 1$ and e_1 is varied between 0.4 and 1; (b) $e_1 = 1$ and e_2 is varied between 0.4 and 1.

and $e(x = 1) = e_2$ for the two limits of a bilayered projectile of total length L. In what follows we keep the total length L constant and restrict the analysis to high rigidity contrast ($\alpha = 0.005$ if not indicated otherwise) with the rigid part at the bottom.

A. Systematic study

The effect of e_1 and e_2 on the coefficient of restitution (Fig. 8) and contact time (Fig. 9) is studied systematically. The case $e_1 = e_2 = 1$ corresponds to dissipative-less projectiles and is characterized by the asymptotes $e(x) = 1 - 2x$ in the limit $x \to 0$ and $e(x) = x$ in the limit $x \to 1$ (Sec. VI). If e_2 is set to 1 while e_1 is varied, the coefficient of restitution keeps approximately the same asymptote at large x and the same initial slope at small x [Fig. 8(a)]. The opposite is observed if e_1 is set to 1 while e_2 is varied [Fig. 8(b)]. The transition zone between the two asymptotes, characterized by strong variations of e, are shifted to larger x if e_2 decreases and to smaller x if e_1 decreases. The effect on the contact time is shown in Fig. 9. In all cases, the two limit regimes are retrieved: $t_c = 2t_1$ for small x and $t_c = 2t_1 + 2t_2$ for large x. Again, the limit between the two regimes is shifted to larger x if e_2 decreases and to smaller x if e_1 decreases.
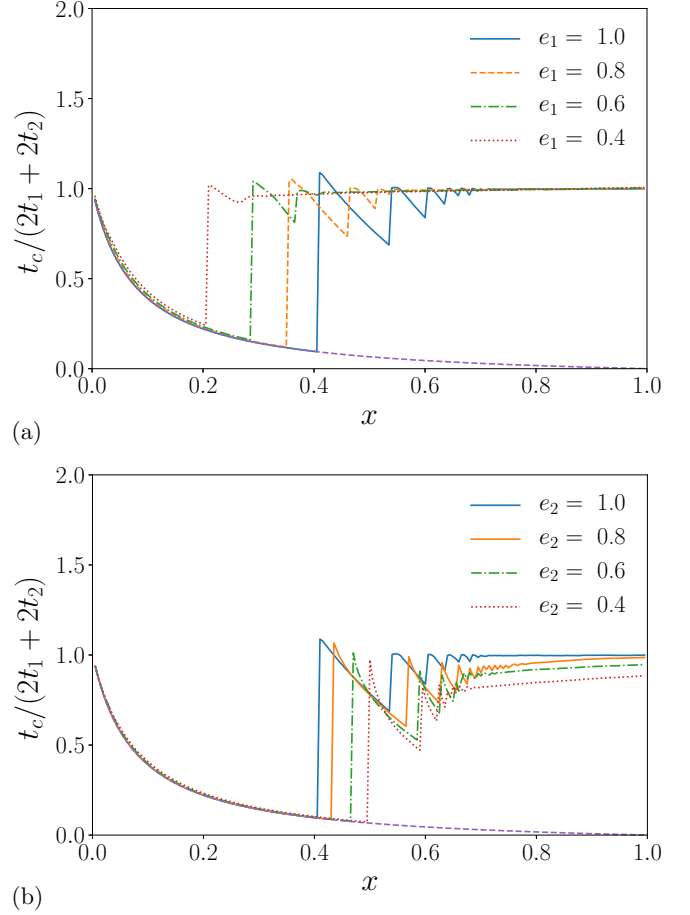

FIG. 9. Dimensionless contact time $t_c/(2t_1 + 2t_2)$ as a function of x for $\alpha = 0.005$: (a) $e_2 = 1$ and e_1 is varied between 0.4 and 1; (b) $e_1 = 1$ and e_2 is varied between 0.4 and 1. The dashed lines correspond to the equation $t_c = 2t_1$.

B. Comparison with experiments

Simulations in the limit $\alpha \to 0$ are compared with experimental data from D'Angelo *et al.* [15] obtained with cylindrical projectiles. The value of $e_1 = 0.94$ and $e_2 = 0.72$ are deduced from experimental measurements by extrapolating the asymptotes in the limits $x \to 0$ and $x \to 1$, respectively. The coefficient of restitution and the number of bounces are shown in Fig. 10. We observe that the agreement is very good for recovering fine details like local variations in e or the staircaselike trend in N_b, although there is no additional fitting parameters.

VIII. DISCUSSION AND CONCLUSION

This one-dimensional numerical study reveals that bilayer elastic projectiles exhibit novel properties when the contrast between the elastic moduli is large and the rigid and soft parts are located at the leading and trailing edges, respectively. This includes the occurrence of multiple bounces and a maximum of absorption for a specific composition ratio. This allows to put in the same context the results obtained with composite objects, either in experiments or in simple models [13,15,16,19]. The absorption can be very strong with
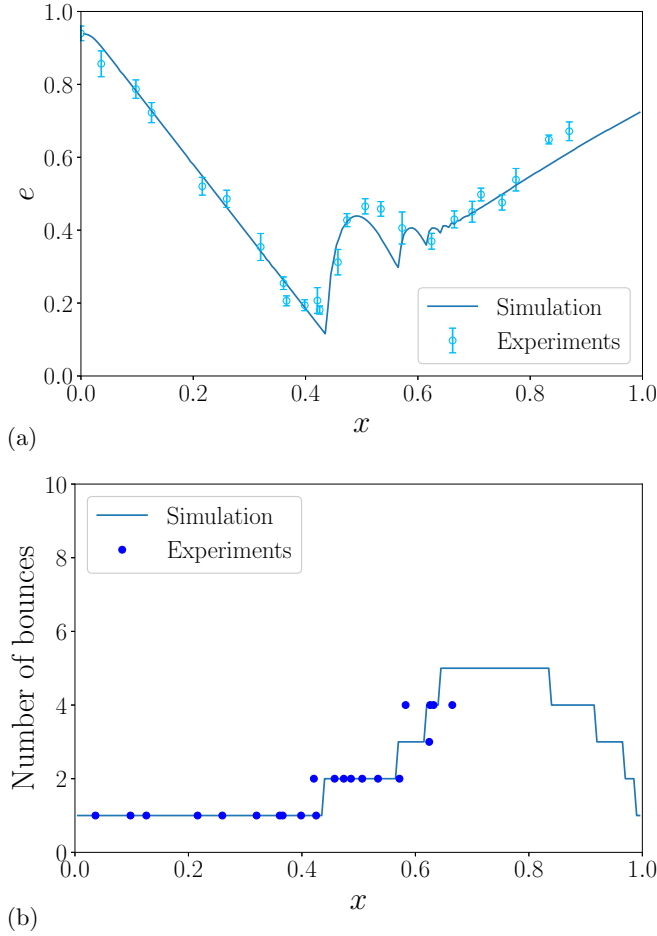
(a)

(b)

FIG. 10. (a) Coefficient of restitution e and (b) number of bounces N_b as functions of x. Simulations are performed in the limit $\alpha \to 0$ and experimental data are taken from D'Angelo *et al.* [15].

a coefficient of restitution as low as 0.2, showing that most of the initial kinetic energy can be trapped in the internal deformation modes if the composition and stiffness ratios are fixed at specific values. In a more general context, this study strengthens the ideas that bilayered elastic objects can exhibit particular properties, very different from the properties of the two parts taken separately, as already shown in ejection experiments [17,18]. Finally, viscoelastic parts can be studied in the same framework and give similar results with a composition ratio at minimum restitution that can be slightly adjusted in either direction by changing the dissipative properties of either part.

ACKNOWLEDGMENTS

APPENDIX A: FINITE-SIZE EFFECTS

In Fig. 11, we observe the coefficient of restitution as a function of the number of elements N for the case of a purely
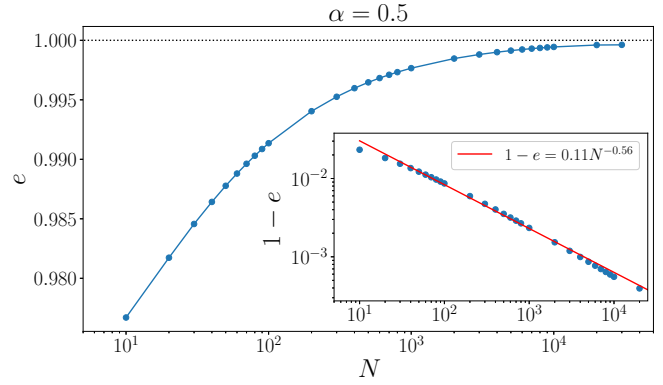

FIG. 11. e as a function of N for $\alpha = 0.5$ and $\tau = 0$. In the inset, $1 - e$ as a function of N in a logarithmic scale. The red line is the best power law fit.

elastic and homogeneous chain ($\alpha = 0.5$ and $\tau = 0$), whose coefficient of restitution is expected to be 1 in theory. We observe that the error is about 1% for $N = 50$. We set this value as the minimum number of elements in a given part. With $\alpha = 0.005$ and 0.995 for the extreme values, this means that taking $N = 10^4$ for the whole chain should keep the error below 1% in all simulations.

APPENDIX B: WAVE APPROACH FOR PURELY ELASTIC PROJECTILES

Three interfaces are found in this problem: the P_1-wall interface at $y = 0$, the P_1-P_2 interface at $y = xL$ and the P_2 free interface at $y = L$. For each of them, velocity and/or force continuity imposes specific conditions for the amplitude of the deformation wave reflected or transmitted at the interface. At the P_1-wall interface [Fig. 12(a)], a wave of amplitude ε traveling with velocity $-c_1$ gives rise to a reflected wave of amplitude ε traveling with velocity $+c_1$. At the P_2 free interface [Fig. 12(b)], a wave of amplitude ε traveling with velocity $+c_2$ gives rise to a reflected wave of amplitude $-\varepsilon$ traveling with velocity $-c_2$. At the P_1-P_2 interface, a wave of amplitude ε traveling with velocity $+c_1$ [Fig. 12(c)] gives rise to a reflected wave of amplitude $R_{12}\varepsilon$ and to a transmitted
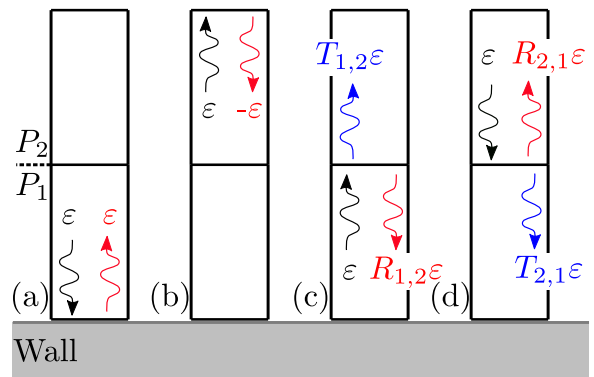

FIG. 12. Descriptive diagram of the reflection and transmission of deformation waves at the interfaces of the projectile. Cases (a)–(d) are described in the text.

wave of amplitude $T_{12}\varepsilon$ traveling with velocity $-c_1$ and $+c_2$, respectively. In addition, a wave of amplitude ε traveling with velocity $-c_2$ [Fig. 12(d)] gives rise to a reflected wave of amplitude $R_{21}\varepsilon$ and to a transmitted wave of amplitude $T_{21}\varepsilon$ traveling with velocity $+c_2$ and $-c_1$, respectively. The reflection and transmission coefficients at this interface are only functions of α and write

$$R_{12}(\alpha) = \frac{\sqrt{\alpha} - \sqrt{1-\alpha}}{\sqrt{\alpha} + \sqrt{1-\alpha}} \text{ and}$$

$$T_{12}(\alpha) = \frac{2(1-\alpha)^{3/2}}{\alpha\sqrt{1-\alpha} + (1-\alpha)\sqrt{\alpha}}, \tag{B1}$$

$$R_{21}(\alpha) = -\frac{\sqrt{\alpha} - \sqrt{1-\alpha}}{\sqrt{\alpha} + \sqrt{1-\alpha}} = -R_{12}(\alpha) \text{ and}$$

$$T_{21}(\alpha) = \frac{2\alpha^{3/2}}{\alpha\sqrt{1-\alpha} + (1-\alpha)\sqrt{\alpha}}. \tag{B2}$$

APPENDIX C: CALCULATIONS IN THE LIMIT $\alpha \to 0$

This Appendix is dedicated to perfectly elastic bilayered projectiles in the limit $\alpha \to 0$ as discussed in Sec. VI C. In this case, $t_1 \ll t_2$ and the lower and stiffer part P_1 can be considered as a rigid and undeformable object. We note y_1, y_2 and v_1, v_2 the position and velocity of the center of mass of the part P_1, P_2 respectively.

Since $t_1 \ll t_2$ the interaction of part P_1 with the wall can be considered as instantaneous and reverses the sign of v_1. Once part P_1 is separated from the wall, it is only subjected to the interaction with P_2 and the dynamics of its center of mass follows $\rho L_1 \frac{dv_1}{dt}(t) = E_2 \partial_{y^+} u(y_c, t)$. As long as the deformation wave does not reach back the $P_1 - P_2$ interface ($t < t_1 + 2t_2 \simeq 2t_2$), the deformation at the interface on the P_2 side writes $\partial_{y^+} u(y_c, t) = -\frac{v_1 + v_b}{c_2}$ [1] and v_1 satisfies

$$\frac{dv_1}{dt} + \frac{v_1}{\tau_{\text{relax}}} = -\frac{v_b}{\tau_{\text{relax}}}, \tag{C1}$$

with $\tau_{\text{relax}} = L_1/c_2$ the relaxation time of this dynamics. We recover the equation of a falling object inside a viscous fluid [15] to describe how the upper part P_2 pushes the lower part P_1 towards the wall. If the object leaves the solid wall with a velocity $v_{1,i}$ at time $t_{1,i}$, the solution of Eq. (C1) during the bounce is written as

$$y_1(t) = L_1/2 + \tau_{\text{relax}}(v_b + v_{1,i})(1 - e^{-(t-t_{1,i})/\tau_{\text{relax}}})$$
$$- v_b(t - t_{1,i}), \tag{C2}$$

with $L_1/2$ the position of the center of mass of part P_1 at contact with the wall. From these considerations, we can build a time sequence of events describing the full motion of the rigid part P_1. At $t = t_{1,1} = 0$, its velocity $v_1(t_{1,1})$ switches from $-v_{1,1} = -v_b$ to $v_{1,1} = v_b$. Between $t_{1,1}$ and $t_{1,2}$, the motion is described by Eq. (C2) until P_1 enters again into contact with the wall at $t = t_{1,2}$ defined by $y_1(t_{1,2}) = L_1/2$. At this instant, its velocity $v_1(t_{1,2})$ switches from $-v_{1,2}$ to $v_{1,2}$ followed again by a motion described by Eq. (C2). This recursive approach leads to the trajectory displayed in Fig. 13(a). We observe that the amplitude of the motion decreases as the number of reconnection/separation stages increases. In Fig. 13(b), $v_{1,i}/v_b$ is plotted as a function of $t_{1,i}/\tau_{\text{relax}}$. It confirms that
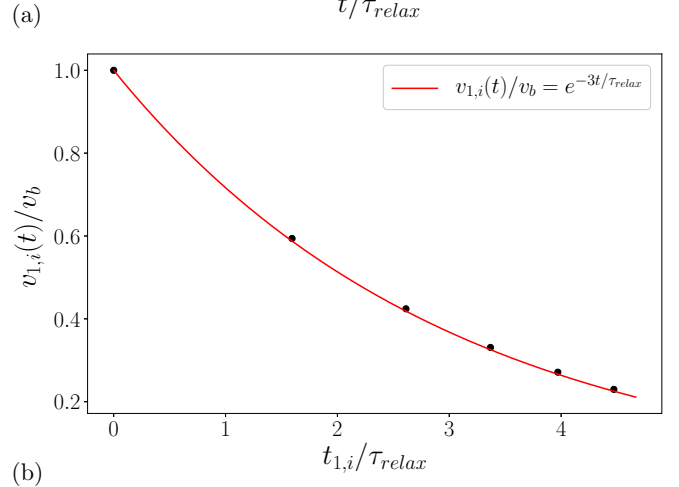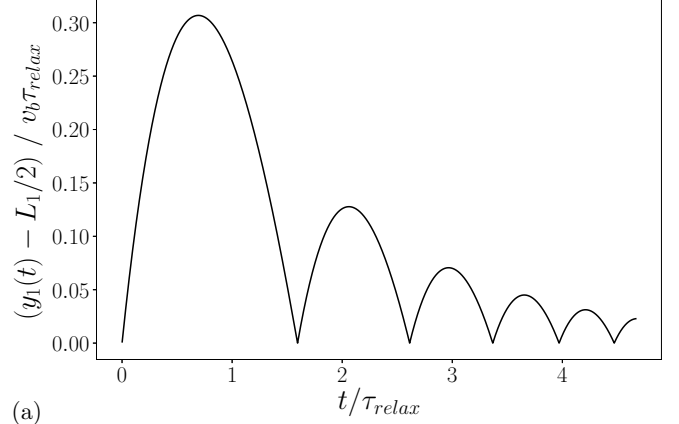

(a)

(b)

FIG. 13. (a) Dimensionless time evolution of the rigid part position as a function of time, as predicted by Eq. (C2). (b) Velocities $v_{1,i}/v_b$ in function of $t_{1,i}/\tau_{\text{relax}}$ (black dots). The red solid line indicates the function $e^{-t_{1,i}/3\tau_{\text{relax}}}$.

the larger i, the smaller $v_{1,i}$ and the smaller the time between two contacts with the wall. Actually, the data can be interpolated with the function $v_{1,i}/v_b = e^{-t_{1,i}/3\tau_{\text{relax}}}$, which shows that the motion of the lower and rigid part P_1 is damped over a characteristic time $3\tau_{\text{relax}}$.

If we perform the same analysis with the part P_2, as long as the deformation waves does not reach back the $P_1 - P_2$ interface, v_2 satisfies

$$\rho L_2 \frac{dv_2}{dt} = E_2 \frac{v_1 + v_b}{c_2}. \tag{C3}$$

Integrating this equation, between 0 and t gives $v_2(t) = -v_b + \frac{y_1(t) - y_1(0)}{t_2} + v_b \frac{t}{t_2}$. This can be used to calculate the coefficient of restitution $e = (1-x)v_1(t_c) + xv_2(t_c)$ with $t_c = 2t_1 + 2t_2 \simeq 2t_2$ in the limit $\alpha \to 0$. Given that the ratio t_c/τ_{relax} is an increasing function of x, the number of reconnection/separation stages is an increasing function of x too. The abrupt changes in the curve $e(x)$ between $x = 0.4$ and 0.7 are thus attributed to changes in the number of reconnection/separation stages [see $\alpha = 0.005$ in Fig. 6(b)]. In the limit $t_2 \gg 3\tau_{\text{relax}}$, we can consider that the motion of the rigid part P_1 is damped so that $v_1(t_c) \simeq 0$ and $y_1(t_c) \simeq y_1(0) = L_1/2$. In this case, we find the expression of an asymptote of the coefficient of restitution, $e(x) = x$, in this limit. Actually,

this asymptote is a good approximation of the coefficient of restitution as long as $t_c \simeq 2t_2 > 3\tau_{\text{relax}}$, which is equivalent to

$L_2 > 1.5L_1$ or $x > 0.6$, in agreement with the behavior of $e(x)$ for $\alpha = 0.005$ in Fig. 6(b).

[1] W. Goldsmith, *Impact* (Edward Arnold, London, 1960).

[2] C. L. Cleveland and U. Landman, Science **257**, 355 (1992).

[3] T. Raz and R. D. Levine, J. Chem. Phys. **105**, 8097 (1996).

[4] W. Christen, U. Even, T. Raz, and R. D. Levine, J. Chem. Phys. **108**, 10262 (1998).

[5] P. U. Andersson and J. B. C. Pettersson, J. Phys. Chem. B **102**, 7428 (1998).

[6] L. Rayleigh, The London, Edinburgh, and Dublin Philosophical Magazine and Journal of Science **11**, 283 (1906).

[7] S. C. Hunter, J. Mech. Phys. Solids **5**, 162 (1957).

[8] J. Reed, J. Phys. D: Appl. Phys. **18**, 2329 (1985).

[9] F. Gerl and A. Zippelius, Phys. Rev. E **59**, 2361 (1999).

[10] H. Kuninaka and H. Hayakawa, J. Phys. Soc. Jpn. **70**, 2220 (2001).

[11] E. Falcon, C. Laroche, S. Fauve, and C. Coste, Eur. Phys. J. B **3**, 45 (1998).

[12] M. Sugiyama and N. Sasaki, J. Phys. Soc. Jpn. **68**, 1859 (1999).

[13] A. G. Basile and R. S. Dumont, Phys. Rev. E **61**, 2015 (2000).

[14] S.-i. Nagahiro and Y. Hayakawa, Phys. Rev. E **67**, 036609 (2003).

[15] C. D'Angelo, L. Viennot, M. Argentina, F. Celestini, and C. Raufaste, Phys. Rev. E **103**, 053005 (2021).

[16] H. Ruan and T. Yu, Int. J. Impact Eng. **88**, 1 (2016).

[17] F. Celestini, J. Mathiesen, M. Argentina, and C. Raufaste, Phys. Rev. Appl. **14**, 044026 (2020).

[18] G. Giombini, J. Mathiesen, C. D'Angelo, M. Argentina, C. Raufaste, and F. Celestini, Phys. Rev. E **105**, 025001 (2022).

[19] C. D'Angelo, L. Viennot, M. Argentina, F. Celestini, and C. Raufaste, Eur. J. Phys. **43**, 065702 (2022).

[20] J. A. Morrison, Q. Appl. Math. **14**, 153 (1956).

[21] D. Beeman, J. Comput. Phys. **20**, 130 (1976).

[22] W. Humphrey, A. Dalke, and K. Schulten, J. Mol. Graphics **14**, 33 (1996).

[23] Y. Berdeni, A. Champneys, and R. Szalai, Proc. R. Soc. A **471**, 20150286 (2015).